

# Probing the Transition State-to-Intermediate Continuum: Mechanistic Distinction between a Dry versus Wet Peroxide in the Singlet Oxygen “Ene” Reaction at the Air–Water Interface

Belaid Malek, Wenchao Lu, Prabhu Prasad Mohapatra, Niluksha Walalawela, Shakeela Jabeen, Jianbo Liu,\* and Alexander Greer\*



Cite This: *Langmuir* 2022, 38, 6036–6048



Read Online

ACCESS |



Metrics & More

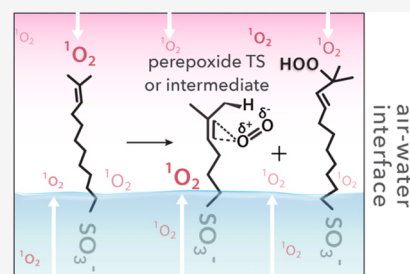


Article Recommendations



Supporting Information

**ABSTRACT:** A mechanistic study is reported for the reactions of singlet oxygen ( $^1\text{O}_2$ ) with alkene surfactants of tunable properties. Singlet oxygen was generated either top-down (photochemically) by delivery as a gas to an air–water interface *or* bottom-up (chemically) by transport to the air–water interface as a solvated species. In both cases, reactions were carried out in the presence of 7-carbon (7C), 9-carbon (9C), or 11-carbon (11C) prenylsurfactants  $[(\text{CH}_3)_2\text{C}=\text{CH}(\text{CH}_2)_n\text{SO}_3^- \text{Na}^+ (n = 4, 6, 8)]$ . Higher “ene” hydroperoxide regioselectivities (secondary ROOH 2 to tertiary ROOH 3) were reached in delivering  $^1\text{O}_2$  top-down through air as compared to bottom-up via aqueous solution. In the photochemical reaction, ratios of 2:3 increased from 2.5:1 for 7C, to 2.8:1 for 9C, and to 3.2:1 for 11C. In contrast, in the bubbling system that generated  $^1\text{O}_2$  chemically, the selectivity was all but lost, ranging only from 1.3:1 to 1:1. The phase-dependent regioselectivities appear to be correlated with the “ene” reaction with photochemically generated, drier  $^1\text{O}_2$  at the air–water interface vs those with wetter  $^1\text{O}_2$  from the bubbling reactor. Density functional theory-calculated reaction potential energy surfaces (PESs) were used to help rationalize the reaction phase dependence. The reactions in the gas phase are mediated by perepoxide transition states with 32–41 kJ/mol binding energy for  $\text{C}=\text{C}(\pi)\cdots^1\text{O}_2$ . The perepoxide species, however, evolve to well-defined stationary structures in the aqueous phase, with covalent C–O bonds and 85–88 kJ/mol binding energy. The combined experimental and computational evidence points to a unique mechanism for  $^1\text{O}_2$  “ene” tunability in a perepoxide continuum from a transition state to an intermediate.



## INTRODUCTION

The singlet oxygen ( $^1\text{O}_2$ ) “ene” reaction with the formation of allylic hydroperoxides is an oxidation reaction of fundamental interest. Whether the  $^1\text{O}_2$  “ene” mechanism proceeds by a concerted or stepwise path has been a point of mechanistic interest and debate. A two-step no-intermediate mechanism has been proposed, suggesting a perepoxide transition state (TS).<sup>1–3</sup> A mechanism involving a perepoxide intermediate has also been proposed.<sup>4–8</sup> In this vein, we have pursued a unique experimental and theoretical approach to evaluate possible *borderline* mechanisms. Our reaction of  $^1\text{O}_2$  with 7-carbon (7C), 9-carbon (9C), and 11-carbon (11C) prenylsurfactants  $[(\text{CH}_3)_2\text{C}=\text{CH}(\text{CH}_2)_n\text{SO}_3^- \text{Na}^+ (n = 4, 6, 8)]$  is now described where the perepoxide (TS *and/or* intermediate) contributes on a continuum to hydroperoxidation, depending on the gaseous or solvated “arrival” of  $^1\text{O}_2$  to the air–water interface (Figure 1).

Our experiments used two reactors, one of which is a photoreactor, and the other a chemical bubbler, wherein  $^1\text{O}_2$  is delivered mainly via gas and solution phases to an air–water interface, respectively. The photo- and bubbling reactors offer a unique way to probe the “ene” reaction mechanism of  $^1\text{O}_2$  at the air–water interface. We hypothesized that by using the air–water interface, the continuum between the two

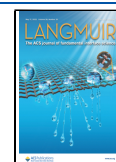
mechanistic extremes of a perepoxide TS vs intermediate will be accessed. Thus, the air–water interface was sought as a novel way to discriminate between concerted and stepwise mechanisms on delivery origin of  $^1\text{O}_2$  to a surface from mainly an upper drier state vs a lower wetter state.

In an effort to accomplish this, methods were required to deliver  $^1\text{O}_2$ . First, a photoreactor was used that isolated the photosensitizer away from the solution to avert type I photooxidation processes that generated *non- $^1\text{O}_2$*  species, such as  $\text{O}_2^{\bullet-}$ ,  $\text{HO}^\bullet$ , and  $\text{ROO}^\bullet$ .<sup>9,10</sup> The photoreactor provided the transmission of  $^1\text{O}_2$  from the upper sensitizer wafer to the air–water interface. Second,  $^1\text{O}_2$  was generated by the chemical reaction of hydrogen peroxide and KOH with chlorine gas bubbled into the solution. This bubbling reactor led to chemically generated  $^1\text{O}_2$ , initially formed as a solvated species.

**Received:** February 2, 2022

**Revised:** April 19, 2022

**Published:** May 4, 2022



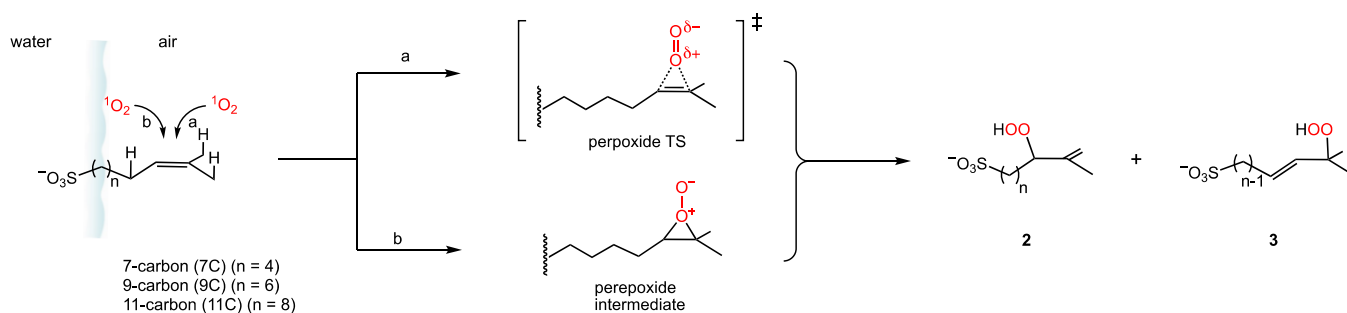


**Figure 1.** Alkene surfactants (7C, 9C, and 11C) were used to probe the “ene” reaction of  $^1\text{O}_2$  at the air–water interface using photoreactor and bubbling devices. The mechanism is proposed to lead to a perepoxide transition state (TS) in the dry state above the air–water interface (path a) and a perepoxide intermediate near the air–water interface or in the aqueous phase (path b), prior to the formation of secondary (2) and tertiary (3) hydroperoxides.

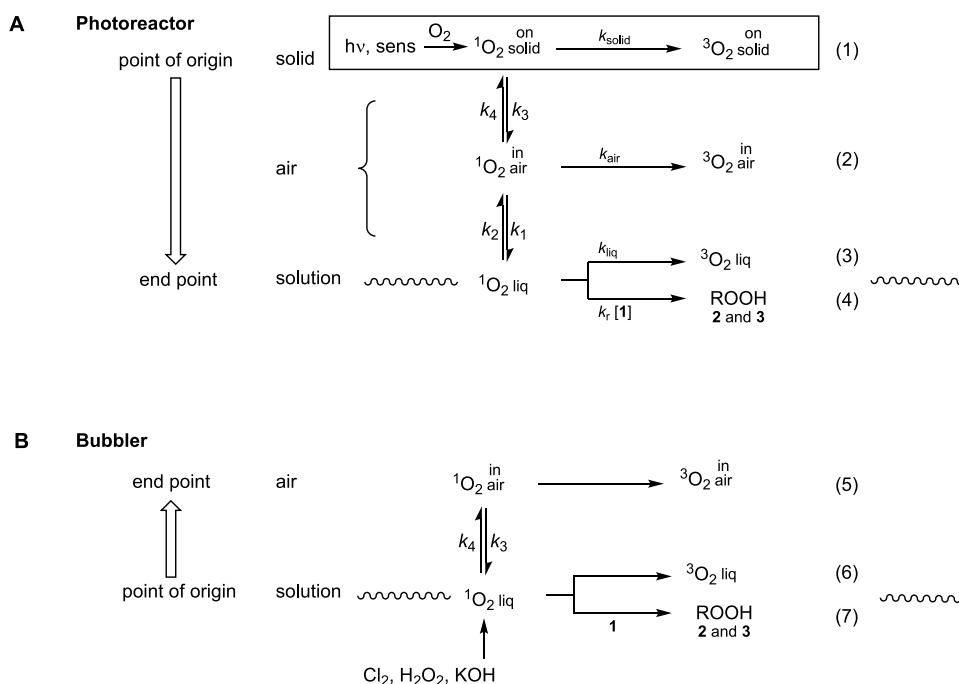


**Figure 2.** (A) A photoreactor *top-down* delivery of  $^1\text{O}_2$  to the air–water interface. We show the formation of  $^1\text{O}_2$  at the sensitizer solid and its physical quenching (eq 1), diffusion through air and its physical quenching in air (eq 2) or by the water surface (eq 3), and chemical reaction with prenylsurfactants 7C, 9C, and 11C to form 7-hydroperoxy-8-methylalkyl-8-ene-1-sulfonate 2 and (*E*)-8-hydroperoxy-8-methylalkyl-6-ene-1-sulfonate 3 (eq 4). For the photoreactor, the surfactant traps  $^1\text{O}_2$  via the gaseous point of origin and then reaches the air–water interface. (B) *Bottom-up* approach of  $^1\text{O}_2$  to the air–water interface. Singlet oxygen was chemically generated by the reaction of  $\text{Cl}_2$  with  $\text{H}_2\text{O}_2$  in KOH solution and transported to the surfactant solution by bubbling for a reaction with 7C, 9C, and 11C to form 2 and 3, leading to a reaction both in solution and at the air–water interface.

Previous studies have also examined  $^1\text{O}_2$  transfer in silicas, zeolites, supramolecular systems, and superhydrophobic surfaces.<sup>11–16</sup> Flow reactors for  $^1\text{O}_2$  generation and reactions in water are emerging and show good potential,<sup>17</sup> as well as surfactants<sup>18–22</sup> in reactive oxygen species (ROS) reactions at the air–water interface.<sup>23–28</sup> A study of Singleton et al.<sup>3</sup> on the reaction of *cis*-2-butene and tetramethylethylene with  $^1\text{O}_2$  proposed a two-step no-intermediate pathway and laid the groundwork for potential bifurcations on the  $^1\text{O}_2$  reaction surface. The *trans*-cyclooctene/ $^1\text{O}_2$  “ene” reaction<sup>29–31</sup> is unique in that its allylic hydrogens are inaccessible so that a minimum develops on the potential energy surface (PES) for the perepoxide. The perepoxide intermediate from the *trans*-cyclooctene/ $^1\text{O}_2$  reaction was predicted by density functional theory (DFT) and trapped experimentally by triphenylphosphite to form *cis*-epoxide, *trans*-epoxide, triphenylphosphate,

and other products. Other  $^1\text{O}_2$  “ene” reactions also show evidence of trapping of a perepoxide intermediate with the formation of epoxides,<sup>32–34</sup> instead of proceeding by a perepoxide TS.

In this study, we report on an air–water interfacial  $^1\text{O}_2$  reaction of alkene surfactants to deduce a possible perepoxide TS-to-intermediate continuum. Figure 2A depicts the top-down approach of  $^1\text{O}_2$  to the air–water interface and its reaction with 7C, 9C, and 11C (eqs 1–4). Figure 2B depicts the bottom-up approach of  $^1\text{O}_2$  to the air–water interface and its reaction with the same surfactants (eqs 5–7). We sought to address the following questions: (i) Does  $^1\text{O}_2$  originating as a gas or in water differ in alkene surfactant oxidation at the air–water interface? (ii) Does a mechanistic difference exist for the oxidation of an alkene surfactant when  $^1\text{O}_2$  is delivered as an airborne species vs solvated state? (iii) Are the regioselectivity

and percent yield of the singlet oxidation affected? (iv) What insight can gas- and aqueous-phase DFT calculations provide on possible borderline perepoxide TS and intermediate mechanisms?

## EXPERIMENTAL SECTION

**General.** Acetone, 9,10-anthracene dipropionate dianion (ADPA), aluminum(III) phthalocyanine chloride tetrasulfonic acid (ALPcS), benzoic acid, Cl<sub>2</sub> gas (≥99.5%), CDCl<sub>3</sub>, D<sub>2</sub>O (99.8%), dichloromethane (DCM), diethyl ether, *N,N*-dimethylformamide (DMF), DMSO-*d*<sub>6</sub> (99.5%), ethanol, ethyl acetate, H<sub>2</sub>O<sub>2</sub> (35 wt %), helium (5 ultra-high purity), and porous Vycor glass (Corning 7930 porous, sized 1.0 mm × 2.25 cm<sup>2</sup>) were obtained commercially and used as received. A deionization system was used to purify water. The syntheses of surfactants 7C and 9C were each carried out in 3 steps in overall yields of 16–27% and purities of 95%, using methods reported in our previous work.<sup>35</sup> The synthesis of sodium 10-methylundec-9-ene-1-sulfonate (11C) was carried out in three steps by slightly modifying our previously reported procedure<sup>35</sup> in an overall yield 100 mg of 60% and purity of 95%. A facet of the photoreactor and bubbling reactor study is that unless otherwise noted, submicellar concentrations of 7C, 9C, and 11C were used, in which no micelles are present in solution.

**Photoreactor.** The photoreactor consisted of a shortened quartz cuvette with a size of 0.7 cm × 1.0 cm<sup>2</sup>. H<sub>2</sub>O or D<sub>2</sub>O (0.60 mL) was placed in the photoreactor that contained either 7C, 9C, or 11C in various amounts. A 0.5 g porous Vycor glass lid of the size 1.0 mm × 2.25 cm<sup>2</sup> was placed on top of the cuvette. ALPcS (5.0 × 10<sup>-6</sup> mol) was coated onto the bottom face of the glass lid. This glass lid generates airborne <sup>1</sup>O<sub>2</sub> on its bottom face, which traveled a 0.4 mm distance relative to the cuvette walls, and a 1.5 mm distance relative to the deepest point of the meniscus, as measured using a digital ruler. The end of a fiber optic was placed 3.0 cm above the glass lid. The fiber optic delivered light from two different laser sources, in which there was a Gaussian distribution of the incident photons. (i) The *k*<sub>T</sub> rate constants for the reaction of airborne <sup>1</sup>O<sub>2</sub> with 7C, 9C, and 11C at the air–D<sub>2</sub>O interface were examined at 26 °C by irradiation from Surelite pulsed Nd:YAG laser using 355 nm light that was connected to a Hamamatsu NIR detector to observe the 1270 nm phosphorescence signal of <sup>1</sup>O<sub>2</sub>. A 1270 nm band-pass filter with a full width at half maximum (FWHM) of 15 nm was used prior to this phosphorescence signal reaching the NIR detector. The lifetime of <sup>1</sup>O<sub>2</sub> (τ<sub>Δ</sub>) as a gaseous species and at the air–D<sub>2</sub>O interface was determined with a least-squares procedure for the curve-fitting. (ii) A continuous-wave diode laser was also used with a 669 nm light output (dose = 1400 J/cm<sup>2</sup>). For both (i) and (ii), the 355 nm and the 669 nm laser outputs overlap well with the ALPcS sensitizer adsorbed on the glass lid. In both cases, airborne <sup>1</sup>O<sub>2</sub> was generated on the bottom face of the lid and proceeded over the air gap to the water interface.

**Bubbling Reactor.** For the bubbling reactor, singlet oxygen was generated on the basis of a chemical reaction of H<sub>2</sub>O<sub>2</sub> + Cl<sub>2</sub> + 2KOH → O<sub>2</sub> (~85% X<sub>3</sub>Σ<sub>g</sub><sup>-</sup> and ~15% a<sup>1</sup>Δ<sub>g</sub>) + 2KCl + 2H<sub>2</sub>O that has been reported previously.<sup>36,37</sup> Briefly, 10.5 mL of 8 M KOH was added to 20 mL of 35 wt % aqueous H<sub>2</sub>O<sub>2</sub> in a glass sparger that was immersed in a chiller held at -17.9 °C. The reaction was mixed with Cl<sub>2</sub> (4.99 mL/min) and He (96 mL/min) within a Matheson gas proportioner and then bubbled through the H<sub>2</sub>O<sub>2</sub>/KOH slush. All of the Cl<sub>2</sub> reacted with H<sub>2</sub>O<sub>2</sub>. The gaseous products passed through a cold trap (kept at -70 °C) to remove the water vapor. Only <sup>1</sup>O<sub>2</sub>, <sup>3</sup>O<sub>2</sub>, and He remained in the downstream gas. The concentration of <sup>1</sup>O<sub>2</sub> in the gas was determined by measuring the <sup>1</sup>O<sub>2</sub> emission (a<sup>1</sup>Δ<sub>g</sub> → X<sub>3</sub>Σ<sub>g</sub><sup>-</sup>, ν = 0–0)<sup>38</sup> at 1270 nm in an optical emission cell. Emission from the cell was collected using a plano-convex BK7 lens (*f* = 30 mm), passed through an optical chopper (SRS model SR540, Sunnyvale, CA, USA) and 5 nm bandwidth interference filter centered at 1270 nm (Andover, blocked to 1550 nm), and focused by another plano-convex BK7 lens (*f* = 50 mm, AR coated for 1050–1620 nm) into a thermoelectrically cooled InGaAs photodetector (Newport model 71887 detector and 77055 TE-cooler controller, Irvine, CA, USA)

coupled with a lock-in amplifier (SRS model SR830, Sunnyvale, CA, USA).

After passing the emission cell, <sup>1</sup>O<sub>2</sub> (mixed with <sup>3</sup>O<sub>2</sub> and He) was bubbled into 10 mL of 1 × 10<sup>-4</sup> M 11C surfactant in a reaction vessel. The solution of 11C was prepared in pure D<sub>2</sub>O, pure H<sub>2</sub>O, or as D<sub>2</sub>O/H<sub>2</sub>O mixtures in volume ratios of 3:1, 1:1, or 1:3. During the experiment, the entire apparatus (including the <sup>1</sup>O<sub>2</sub> generator and the reaction vessel) was continuously pumped using a mechanical pump, and the pressure of the apparatus was maintained at 26 Torr (slightly above the water vapor pressure at room temperature) through a pressure relay (Cole-Parmer 00244OW, Vernon Hills, IL, USA). The pumping served several purposes: it reduced the residence time of <sup>1</sup>O<sub>2</sub> in the gas phase, thus minimizing its wall quenching and self-quenching, and removed O<sub>2</sub>, thus replenishing fresh <sup>1</sup>O<sub>2</sub> to the reaction solution. Because of the low pressure within the reaction vessel, a significant amount of solvent evaporated from the reaction solution and was removed by the vacuum pump. Fresh solvent (with the same D<sub>2</sub>O/H<sub>2</sub>O composition as the original solution) was replenished into the reaction vessel using an Ismatec Reglo-CPF rotary piston pump (Glattbrugg, Switzerland) at a precisely controlled flow rate, so that the total volume of the solution remained constant throughout the reaction.

In the experiment, chemically generated <sup>1</sup>O<sub>2</sub> was continuously bubbled into the aqueous solution in the reaction vessel. Singlet oxygen has a longer lifetime in the interior of bubbles (because of reduced encounters with water) than in the bulk solution. After diffusing into the bulk water, <sup>1</sup>O<sub>2</sub> has a lifetime of ~4 μs and can travel only ~150 nm.<sup>39,40</sup> Therefore, <sup>1</sup>O<sub>2</sub> reactions occurred both at the gas–liquid interface of bubbles and in the bulk solution. ADPA was used as a <sup>1</sup>O<sub>2</sub> trap to estimate the average [<sup>1</sup>O<sub>2</sub>] in solution. ADPA is known to react with <sup>1</sup>O<sub>2</sub> chemically (i.e., without physical quenching), producing endoperoxide via [4 + 2] cycloaddition accompanied by bleaching of the absorption of ADPA.<sup>41</sup> The pH of the ADPA solution (0.05 mM) was maintained at 10 using borax/NaOH buffer. A linear relationship between ln(A<sub>t</sub>/A<sub>0</sub>) and reaction time was observed,<sup>37</sup> where A<sub>t</sub> and A<sub>0</sub> are the ADPA peak absorption (at 378 nm) at different reaction times and time zero, respectively. This indicates that the consumption of ADPA obeys the first-order rate law. Using the literature value of reaction rate constant *k*<sub>t</sub> (8.2 × 10<sup>-7</sup> M<sup>-1</sup> s<sup>-1</sup>) for ADPA + <sup>1</sup>O<sub>2</sub>, the average concentration of <sup>1</sup>O<sub>2</sub> in solution was determined to be ~5–7 × 10<sup>-12</sup> M. During each experiment, the emission of airborne <sup>1</sup>O<sub>2</sub> was continuously monitored, and its variation was controlled to be within 10%. It was found that the average signal output of the emission detector linearly correlates with the ADPA-calibrated [<sup>1</sup>O<sub>2</sub>] in solution. Therefore, in the experiment of 11C surfactants with <sup>1</sup>O<sub>2</sub>, [<sup>1</sup>O<sub>2</sub>] in water was determined based on a calibration curve for the gas-phase emission intensity vs solution-phase concentration.

**Computations Details.** DFT electronic structure calculations were performed using B3LYP coupled with the 6-31+G(d) basis set. Geometries of reactants, TSs, intermediates, and products were fully optimized by calculating force constants at every step. TSs were verified as first-order saddle points by frequency calculations, and the vibrational mode with the imaginary frequency corresponds to the reaction coordinate. Intrinsic reaction coordinate calculations were carried out to further verify that each TS was connected to the correct reactant/product minima. Reaction enthalpies reported for each pathway included thermal corrections at 298 K, for which the zero-point energies were scaled by a factor of 0.9804.<sup>42</sup> The reactions in aqueous solution were calculated using the SMD solvation model.<sup>43</sup> For a relaxed PES scan, all bond lengths and bond angles were fully optimized at each step, except for the two scanning reaction coordinates, which were each varied continuously from 2.5 to 1.4 Å at a step size of 0.1 Å.

One challenge in the DFT calculations concerns the multi-configurational <sup>1</sup>O<sub>2</sub> wave function that mixes open- and closed-shell characters.<sup>44</sup> The spin-restricted DFT is incapable of treating static correlation arising from the two degenerate π\* antibonding orbitals and overestimates the <sup>1</sup>O<sub>2</sub> excitation energy, while the broken-symmetry, spin-unrestricted DFT brings about spin contamination

from  $^3\text{O}_2$ . The problem exists not only in the  $^1\text{O}_2$  reactant but may also affect the loosely bonded  $\text{O}_2$  adducts (such as a reactant-like precursor complex without a covalent bond and with a large amplitude of intermolecular motions).<sup>45</sup> To assess the influence of spin contamination on the reaction PES, the B3LYP/6-31G+(d)-optimized  $^1\text{O}_2$  and  $\text{O}_2$ -adduct structures were subjected to a T1 diagnostic of Lee and Taylor<sup>46</sup> using the domain-based local pair-natural orbital coupled-cluster single-, double-, and perturbative triple-excitation method<sup>47</sup> DLPNO-CCSD(T) coupled with the aug-cc-pVTZ basis set, wherein  $T_1 = t_1/\sqrt{n}$  (i.e., the Frobenius norm of the single-excitation amplitude vector divided by the square root of the number of electrons correlated). The inclusion of a perturbative correction for triple excitation in CCSD(T) compensated for the deficiencies of a single-determinant reference to some extent. Empirically, a  $T_1$  value that is greater than 0.02 for a closed-shell system or greater than 0.03 for an open-shell system indicates severe multiconfigurational characters or nondynamical correlation effects. For all reactive structures including  $^1\text{O}_2$ , the  $T_1$  values do not exceed 0.018. Accordingly, spin contamination does not appear to be a significant issue for the present reaction system. DFT calculations were carried out using Gaussian 09.<sup>48</sup> DLPNO-CCSD(T) calculations were conducted by using ORCA 4.2<sup>49</sup> at a Linux computational cluster equipped with 20 nodes of dual Intel Xeon 28-core 2.7 GHz processors.

## RESULTS AND DISCUSSION

**Apparatus.** Two apparatuses were used to probe the “ene” reaction of  $^1\text{O}_2$  at the air–water interface, as shown in Figure 3. First, an apparatus previously described<sup>35,50,51</sup> was equipped with a porous glass wafer coated with Al(III) phthalocyanine chloride tetrasulfonic acid as the sensitizer on its bottom face, and a reactor loaded with surfactant on the solution was irradiated from above with red light via an optical fiber. Singlet oxygen traverses an air-gap distance of 0.4 mm from the sensitizer plate to the water surface at the walls of the cuvette and further to the meniscus. Second, a bubbling system previously described<sup>36,37</sup> led to  $^1\text{O}_2$  by a chemical reaction of  $\text{Cl}_2$  gas with  $\text{H}_2\text{O}_2$  in a basic solution. Here, much of  $^1\text{O}_2$  was distributed through water via bubbles. Next, the results from the use of these two techniques are presented.

The results are presented as follows: (1) the total quenching rate constants ( $k_T$ ) for the removal of  $^1\text{O}_2$  by the surfactants; (2) analysis of the device geometry on hydroperoxide product yield; (3) the regioselectivity of hydroperoxides based on the chain length; (4) effect of solvent deuteration; (5) the sorting out of DFT-computed gas- and water-phase contributions to the  $^1\text{O}_2$  “ene” reaction; and (6) mechanistic considerations.

**Effect of the Chain Length on  $k_T$ .** With the advent of a technique to monitor the quenching of  $^1\text{O}_2$  at the air– $\text{D}_2\text{O}$  and air–solid interfaces,<sup>16,51</sup> the rate constants  $k_T$  can show the removal of  $^1\text{O}_2$  by the surfactants. In the present  $k_T$  experiments, the use of  $\text{D}_2\text{O}$  was preferred because of a longer lifetime in  $\text{D}_2\text{O}$  ( $\tau_\Delta = 66 \mu\text{s}$ ) than in  $\text{H}_2\text{O}$  ( $\tau_\Delta = 4.5 \mu\text{s}$ ),<sup>52</sup> thereby facilitating the time-resolved measurements. Consequently, surfactants 7C, 9C, and 11C provide the first opportunity to measure the removal of  $^1\text{O}_2$  to assess the chain length on the rate constant at the air–water interface. The interfacial effect on the  $k_T$  of  $^1\text{O}_2$  was measured by monitoring the ability of alkene surfactants 7C, 9C, and 11C to quench the phosphorescence of  $^1\text{O}_2$  at 1270 nm, as shown in eq 4 (Figure 2). Among the two decay components observed in the 1270 nm  $^1\text{O}_2$  phosphorescence, there was a slow component corresponding to  $^1\text{O}_2$  in the air space and a fast component ascribed to  $^1\text{O}_2$  at the air– $\text{D}_2\text{O}$  interface. The  $k_T$  of  $^1\text{O}_2$  of 9C was previously measured to be  $1.1 \times 10^6 \text{ M}^{-1} \text{ s}^{-1}$  at the air/

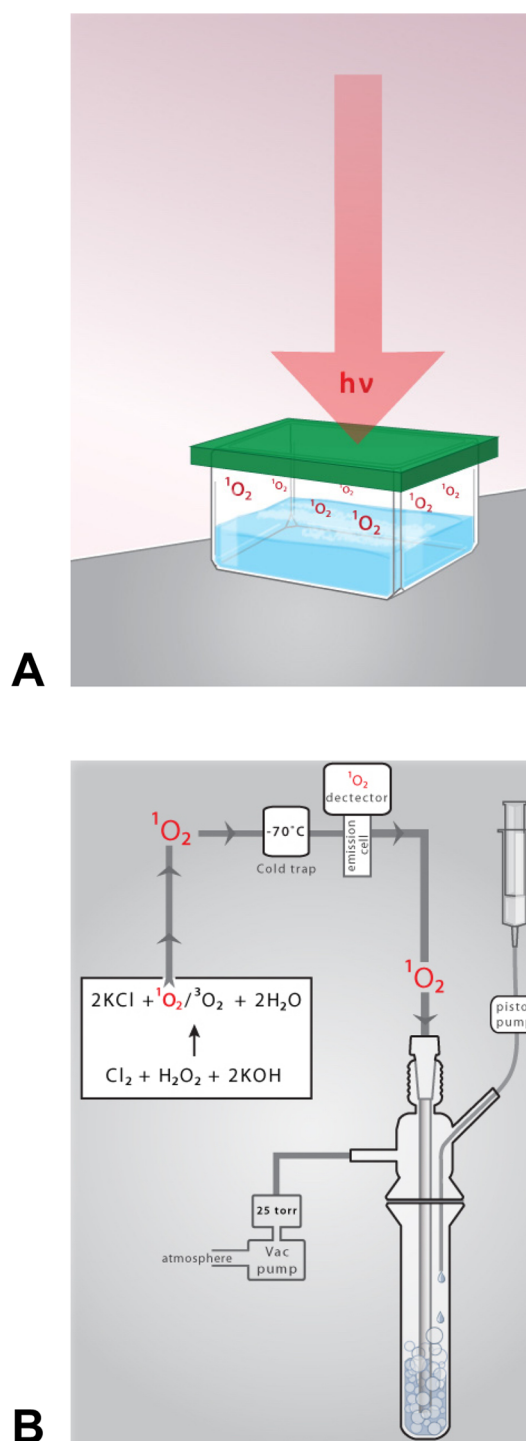


**Figure 3.** (A) Top-down approach of the photoreactor with delivery of  $^1\text{O}_2$  to the air–water interface. (B) Bottom-up approach of  $^1\text{O}_2$  to the air–water interface with the chemical generation of  $^1\text{O}_2$ .

liquid interface.<sup>51</sup> We find that quenching of the phosphorescence of  $^1\text{O}_2$  at the air/ $\text{D}_2\text{O}$  interface produces  $k_T$  values that are increased by 2.7-fold for 11C compared to 9C, and 4.6-fold for 11C compared to 7C (Figure 4 and Table 1). These interfacial  $k_T$  values are similar to homogeneous solution  $k_T$  values reported for trisubstituted alkenes,<sup>53,54</sup> in which increasing the surfactant chain length, from 7C to 11C, increased not only the  $k_T$  of  $^1\text{O}_2$  for the prenylsurfactants but

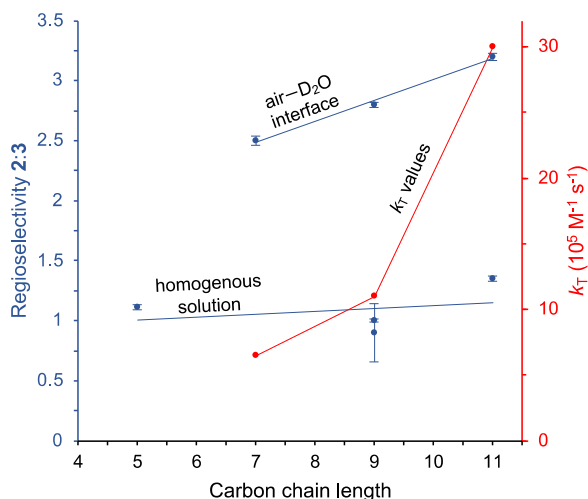


**Figure 4.** A plot of regioselectivity in forming 2:3 (upper blue ● trendline  $y = 0.175x + 1.26$ ,  $R^2 = 0.993$ ) and total quenching rate constant  $k_T$  (red ●) vs alkene chain length of surfactants 7C, 9C, and 11C upon the delivery of  $^1\text{O}_2$  to the air– $\text{D}_2\text{O}$  interface. Regioselectivity in forming 2:3 (lower blue ● trendline  $y = 5.87x - 37.0$ ,  $R^2 = 0.0908$ ) alkene chain length, and surfactants 9C and 11C of  $^1\text{O}_2$  in homogeneous solution  $\text{CD}_3\text{CN}/\text{D}_2\text{O}$  (9:1). The  $k_T$  of 2-methyl-2-pentene is taken from ref 53.

also the percent yield of hydroperoxides from “ene” reactions, as we will see next.

**Effect of Device Geometry on the Hydroperoxide Product Yield.** The percent yield of the hydroperoxide products 2 and 3 was investigated based on configurations of the  $^1\text{O}_2$  apparatus. Table 1 shows the results that were collected for the photoreactor (entries 1–3, 9, and 10) and bubbler (entries 4–8) systems. For the photoreactor with  $\text{D}_2\text{O}$ , as the surfactant chain length increases from 7C to 11C, an increase in the hydroperoxide percent yield from 75 to 85% was observed. The percentage yield of hydroperoxides for 11C in the photoreactor was 85% and in the bubbler was 67.4% (cf. entries 1 and 4); this reduction is attributed to greater solvation in the latter. The effect of solvent deuteration is evident in the bubbler reactor, and the hydroperoxide percent yield was decreased from 67.4% in  $\text{D}_2\text{O}$  to 31.3% in  $\text{H}_2\text{O}$  (cf. entries 4 and 8). For the photoreactor, 11C in a micellar condition shows a loss of the regioselectivity (entry 9), suggesting that the reaction of airborne  $^1\text{O}_2$  reaches the water phase, which then enters a hydrophobic core similar to the homogeneous phase. The arrival of airborne  $^1\text{O}_2$  to a solution interface with alkene surfactant sites solvated also in “on water/ $\text{CD}_3\text{CN}$ ” organic reaction (entry 10) also led to a loss of regioselectivity, indicating the need for the interaction of  $^1\text{O}_2$  with the alkene site positioned above the air–water interface (entries 1–4). The regioselectivity of the surfactant– $^1\text{O}_2$  “ene” reaction was also investigated based on the  $^1\text{O}_2$  apparatus, as described next.

**Effect of the Chain Length on the Regioselectivity of the “Ene” Reaction.** The prenylsurfactants reacted with  $^1\text{O}_2$  to give two “ene” hydroperoxides 2 and 3 in varying ratios. For the photoreactor, the product ratios of 2:3 decreased from  $3.2 \pm 0.03$  for 11C, to  $2.8 \pm 0.02$  for 9C, and to  $2.5 \pm 0.04$  for 7C (entries 1–3). The regioselectivity is all but lost in the bubbler compared to the photoreactor. For the bubbler reactor, the regioselectivity ranged from 1.35:1 to 1.04:1 (entries 4–8). The micelle or solution phase ranged from 0.9:1 to 1.11:1

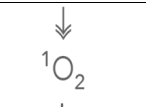
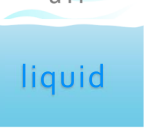
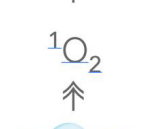
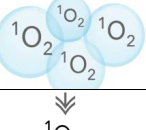
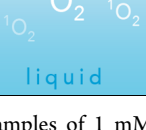
(entries 9–11). There is little or no regioselectivity in the solvated state. In homogeneous solution,  $^1\text{O}_2$  “ene” reactions show little or no preference, where 2 and 3 are formed in nearly equal amounts. A complete loss of regioselectivity when 9C is dissolved in a homogeneous solution, as has been observed for 2-methyl-2-pentene in organic solvents (entries 10 and 11). Next, our analysis shows the reactivity of 11C with  $^1\text{O}_2$  with various compositions of  $\text{D}_2\text{O}$  vs  $\text{H}_2\text{O}$ .

**Effect of Solvent Deuteration.** Experiments were conducted to quantitate the percent yield of hydroperoxides 2 and 3 in the reaction of 11C. Table 1 shows that the percent yield of the hydroperoxides increased by  $\sim 2$ -fold in  $\text{D}_2\text{O}$  compared to  $\text{H}_2\text{O}$  (67.4% in  $\text{D}_2\text{O}$  and 31.3% in  $\text{H}_2\text{O}$ , entries 4 and 8). We find that 11C’s chemical reactivity does not increase by 20-fold as would be expected for aqueous solvated species with the known longer  $^1\text{O}_2$  lifetime in  $\text{D}_2\text{O}$  compared to  $\text{H}_2\text{O}$ .<sup>52</sup> Thus, the results are consistent with the partial solvation of 1 and point to a dependence on mixing rates, as will be seen next.

**Effects of Gas and Water Phases Based on DFT Calculations. Gas-Phase Calculations wherein All Structures Are Dry.** When  $^1\text{O}_2$  attacks the 11C surfactant in a *cis* orientation in the gas phase, a perepoxide structure forms as a TS (Figure 5a). The reaction follows Singleton and coworkers’ two-step no-intermediate mechanism.<sup>3</sup> Both TS1 and TS2 in Figure 5a are located in energy below the reactants. The energy gap between TS1 and TS2 is 12 kJ/mol calculated at B3LYP/6-31+G(d). Singlet oxygen attacks the  $\pi$  bond nearly symmetrically, as shown by the close distances of R2 and R3 in TS1 (R2 = 2.07 Å and R3 = 2.16 Å). The 2° hydroperoxide is a less-stable *anti*-Markovnikov product, while the 3° hydroperoxide is a more stable Markovnikov product. According to the two-dimensional (2D)-PES shown in the top left frame of Figure 6, a longer route is required to reach the 2° ROOH compared to that for the 3° ROOH. For the comparison of the reaction of 11C with that of a short-chain species, the PES for the  $^1\text{O}_2$  reaction with 2-methyl-2-butene in the gas phase was calculated as well. It also shows a two-step no-intermediate process, consistent with the results of Singleton et al.<sup>3</sup> The perepoxide complex could also be characterized as a loosely bound perepoxide when  $^1\text{O}_2$  attacks the 11C surfactant in a *trans* orientation. As shown in Figure 5b, the binding strength of such a  $^1\text{O}_2$  complex is 32 kJ/mol at B3LYP/6-31+G(d). Considering that the B3LYP calculation may be affected by the spin contaminations arising from the  $^1\text{O}_2$  reactant and its adducts, we have refined the gas-phase reaction energetics using the domain-based local pair-natural orbital coupled-cluster single-, double-, and perturbative triple-excitation method<sup>47</sup> with DLPNO-CCSD(T) coupled with the aug-cc-pVTZ basis set. The inclusion of a perturbative correction for triple excitation in CCSD(T) enables to some extent a compensation for the deficiencies of a single-determinant reference. The corrections of the PES energies at the CCSD(T) level of theory are overall minor. The major revision by the CCSD(T) theory is that the gas-phase transition states TS1 and TS2 for the gas-phase *cis* reaction are both below the starting reactants, while the TS3 for the gas-phase *trans* reaction increases up to 2 kJ/mol above the starting reactants. This rationalizes (to some extent) the experimentally observed *cis*-effect.<sup>5</sup>

**Water-Phase Calculations wherein All Structures Are Fully Solvated.** Different from the gas-phase scenario, the perepoxide of the 11C surfactant exists as an intermediate

Table 1. Effects of Surfactant Mixing on the Percent Yield and Ratio of Hydroperoxides 2 and 3 Formed by Ene  $^1\text{O}_2$  Reactions

entry	compound	method		$^1\text{O}_2$		% yield (2 + 3)	product ratio 2/3	$k_T$ $\text{M}^{-1}\text{s}^{-1}$
		carbon chain length	solvation state	interfacial	solvent			
1 <sup>a</sup>	undecene-sulfonate	11	$^1\text{O}_2$ air–water not solvated		D <sub>2</sub> O	85 ± 2 <sup>c</sup>	3.2 ± 0.03 <sup>c</sup>	3.0 × 10 <sup>6</sup>
2 <sup>a</sup>	nonene-sulfonate	9	$^1\text{O}_2$ air–water not solvated		D <sub>2</sub> O	81 ± 2 <sup>c</sup>	2.8 ± 0.02 <sup>c</sup>	1.1 × 10 <sup>6,d</sup>
3 <sup>a</sup>	heptene-sulfonate	7	$^1\text{O}_2$ air–water not solvated		D <sub>2</sub> O	75 ± 3 <sup>c</sup>	2.5 ± 0.04 <sup>c</sup>	6.5 × 10 <sup>5</sup>
4 <sup>b</sup>	undecene-sulfonate	11	$^1\text{O}_2$ solvated		D <sub>2</sub> O	67.4 <sup>e</sup>	1.35 ± 0.02	-
5 <sup>b</sup>	undecene-sulfonate	11	$^1\text{O}_2$ solvated		D <sub>2</sub> O:H <sub>2</sub> O 3:1	64.3 <sup>e</sup>	1.04	-
6 <sup>b</sup>	undecene-sulfonate	11	$^1\text{O}_2$ solvated		D <sub>2</sub> O:H <sub>2</sub> O 1:1	54.9 <sup>e</sup>	1.30	-
7 <sup>b</sup>	undecene-sulfonate	11	$^1\text{O}_2$ solvated		D <sub>2</sub> O:H <sub>2</sub> O 1:3	42.5 <sup>e</sup>	1.34	-
8 <sup>b</sup>	undecene-sulfonate	11	$^1\text{O}_2$ solvated		H <sub>2</sub> O	31.3 <sup>e</sup>	1.31	-
9 <sup>f</sup>	nonene-sulfonate	9	micelle		H <sub>2</sub> O	25 ± 6	0.9 ± 0.2	-
10 <sup>g</sup>	nonene-sulfonate	9	solvated		aqueous CD <sub>3</sub> CN	100 ± 1	1.0 ± 0.01	-

<sup>a</sup>Airborne  $^1\text{O}_2$  was generated by the photoreactor for 1 h. Samples of 1 mM surfactant were in 0.6 mL of D<sub>2</sub>O (submicellar concentration).

<sup>b</sup>Bubbler introduced  $^1\text{O}_2$  from a reaction of Cl<sub>2</sub>, H<sub>2</sub>O<sub>2</sub>, and KOH for 1 h. Samples of 1 mM surfactant in 3 mL (submicellar concentration). <sup>c</sup>Ref 35. <sup>d</sup>Ref 51. <sup>e</sup>Errors are ±1%. <sup>f</sup>Airborne  $^1\text{O}_2$  was generated by the photoreactor for 1 h. Samples of 25 mM surfactant were in 0.6 mL of H<sub>2</sub>O (micellar concentration). <sup>g</sup>Airborne  $^1\text{O}_2$  was generated by the photoreactor for 1 h. Samples of 1 mM surfactant were in 0.6 mL of CD<sub>3</sub>CN/D<sub>2</sub>O (9:1).

complex in aqueous solution regardless of the  $^1\text{O}_2$ -approaching orientations, as shown by 1D reaction PESs in Figure 7 and relaxed 2D-PESs in Figure 8. The binding energies of the *cis*-/*trans*-peroxides are 85–88 kJ/mol in water and is more strongly bonded than the gas-phase analogous. The solution-phase reaction follows Acevedo and co-workers' *cis*- and *trans*-peroxide intermediate mechanism. It should be noted that DFT PES implies that the formation of the 2° ROOH is more

favored as it can be formed via both *cis*- and *trans*-peroxide intermediates. The gas-phase peroxide TSs have long C–O bonds (R2 = 1.8–2.4 Å and R3 = 1.6–2.2 Å). In contrast, the solvated peroxide intermediate contains shorter C–O bonds (R2 = 1.5 Å and R3 = 1.6 Å). The latter is anticipated for decreased  $\pi$ -bond character, which is similar to the C–O bond lengths of epoxides (~1.47 Å).

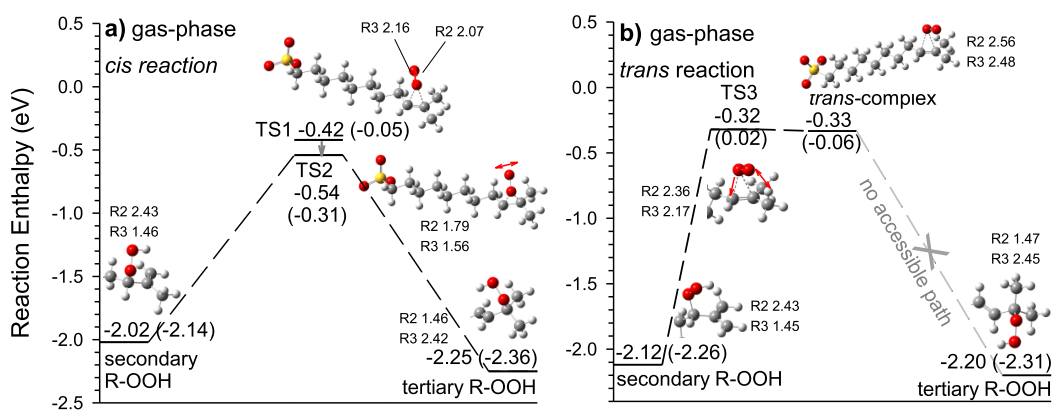


**Figure 5.** Reaction coordinates for the  $^1\text{O}_2$  oxidation of the 11C surfactant in the gas phase, occurring in (a) a *cis*-orientation and (b) a *trans*-orientation. Reaction enthalpies (relative to the corresponding reactants) were calculated at B3LYP/6-31+G(d) and DLPNO-CCSD(T)/aug-cc-pVTZ (values listed in parenthesis), both of which include thermal corrections at 298 K. For most structures, only the portions participating in reactions are depicted. For TSs, vibrational modes corresponding to imaginary frequencies are indicated by displacement vectors. Bond lengths are indicated in the unit of angstrom.

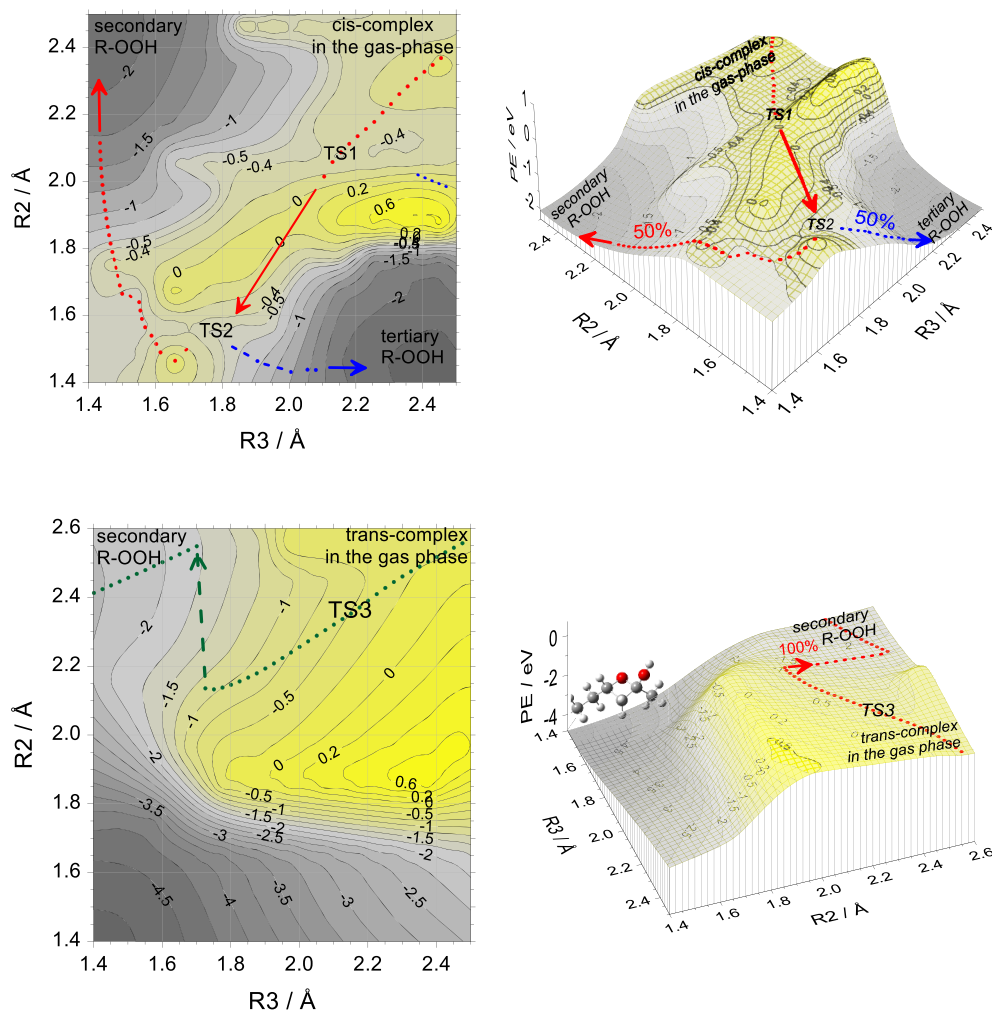


**Figure 6.** Relaxed 2D-PES scan along the R2 and R3 bond lengths (see definitions in Figure 5) of (top) a *cis*-reaction formed in the gas phase, which leads to the formation of both secondary and tertiary hydroperoxides (indicated by dotted lines) via the same transition state TS2 and thus with equal possibilities; (bottom) a *trans*-reaction formed in the gas phase, which exclusively evolves to a secondary hydroperoxide via TS3 (indicated by dotted line). Numbers in the contour map are the potential energies calculated at the B3LYP/6-31+G(d) level of theory.

**Mechanistic Considerations.** The mechanism that we propose is based on an  $^1\text{O}_2$  interfacial effect in the partitioning of the perepoxide toward a TS or an intermediate. Our DFT

computations provide evidence for borderline mechanisms, in which the perepoxide is a transition state in the gas phase while an intermediate in the water phase. These DFT-computed

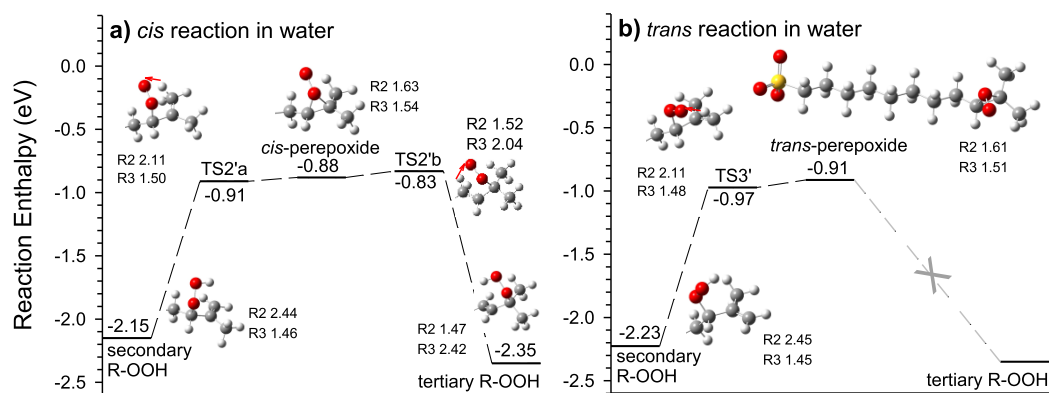


**Figure 7.** B3LYP/6-31+G(d)-computed reaction coordinates for the  $^1\text{O}_2$  oxidation of the 11C surfactant in water, mediated by (a) a *cis*-perepoxide and (b) a *trans*-perepoxide. Reaction enthalpies are relative to the corresponding reactants and include thermal corrections at 298 K. Water solvation effects were calculated using the PCM model. For most structures, only the portions participating in reactions are depicted. For TSs, vibrational modes corresponding to imaginary frequencies are indicated by displacement vectors. Bond lengths are indicated in the unit of angstrom.

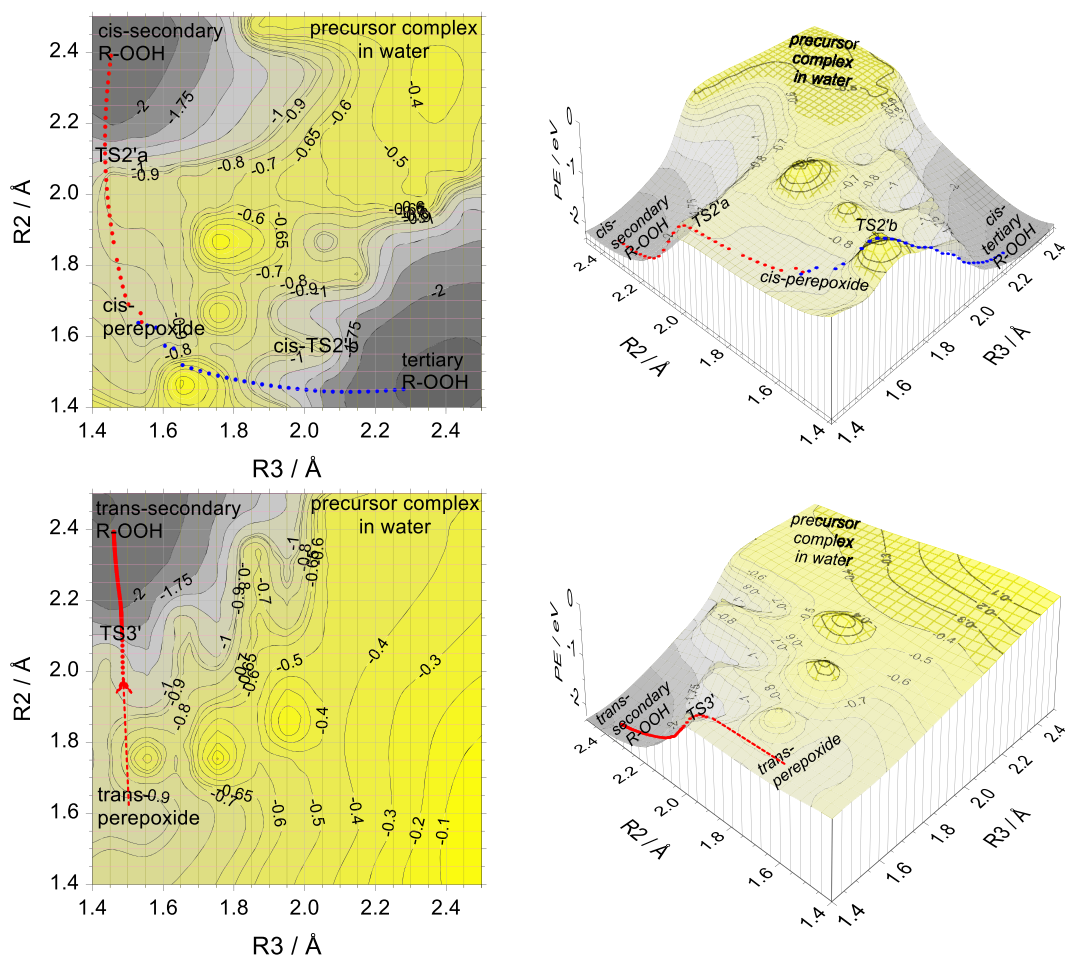


**Figure 8.** Relaxed 2D-PES scan along the R2 and R3 bond lengths (see definition in Figure 7) of (top) a *cis*-perepoxide formed in solution, which leads to secondary and tertiary hydroperoxides via TS2'a and TS2'b, respectively; the two product channels have nearly equal activation barriers, with the secondary hydroperoxide being slightly favored; (bottom) a *trans*-complex formed in solution, which evolves exclusively to secondary hydroperoxide via TS3'. Numbers in the contour map are the potential energies calculated at the B3LYP/6-31+G(d) level of theory.

results combined with the experimental results in the photoreactor and bubble reactor provide evidence for the formation of perepoxide in a continuum from the TS to the intermediate. The data with interfacial effects are reminiscent of structure effects provided by strained alkenes, in which cases, the allylic proton in *trans*-cyclooctene is remote and out

of the proper position for abstraction by  $^1\text{O}_2$ , thereby enabling the formation of a perepoxide intermediate.<sup>29,30</sup> The DFT-computed initial interaction of  $^1\text{O}_2$  at the alkene site of 11C is sensitive to the gas phase as the perepoxide TS is very weakly bound with a strength of only 32–41 kJ/mol with long C–O bonds of 1.8–2.4 Å. This situation changes in aqueous

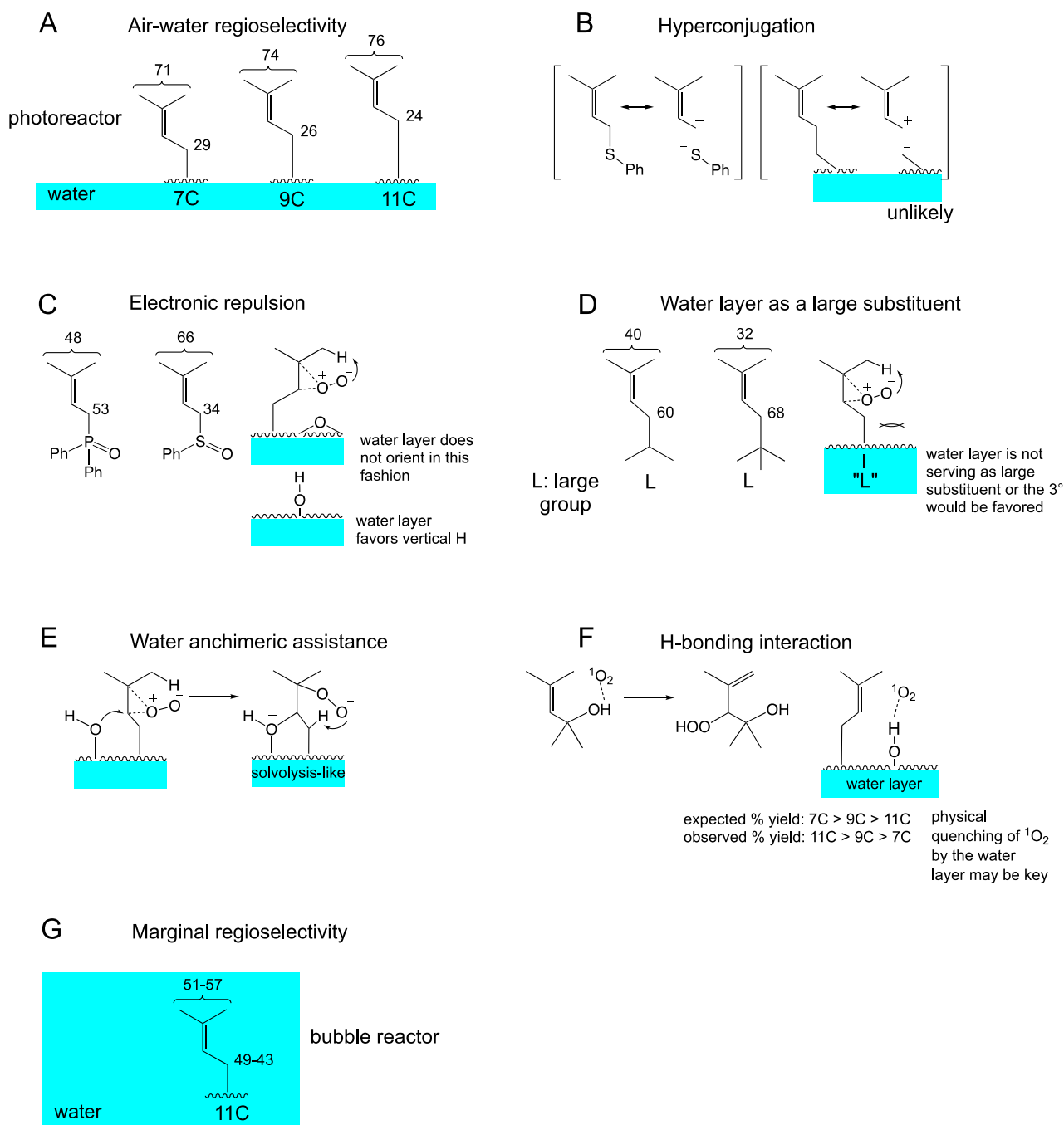


**Figure 9.** Possible mechanisms to account for the regioselectivity observed in the reaction of surfactants with  $^1\text{O}_2$  at the air–water interface.

solution, in which the peroxide intermediate is bound with a higher strength of 85–88 kJ/mol with shorter C–O bonds of 1.5–1.6 Å and bears a resemblance to typical C–O bond lengths of epoxides.

To provide evidence for the variable reactivity of  $^1\text{O}_2$  to the air–water interface, the singlet oxygenations by the photoreactor and the bubble reactor in the presence of surfactants were of use. In the photoreactor, higher hydroperoxidation yields were observed as the surfactant length increased. We attributed this increased product yield to the enhanced contact between the alkene group and  $^1\text{O}_2$  in the air gap from longer surfactants. In the bubble reactor, replacing the solvent  $\text{H}_2\text{O}$  for  $\text{D}_2\text{O}$  led to a 2.1-fold increase of the reaction yield of 11C, which is less than the 20-fold increase that would be expected

when  $^1\text{O}_2$  is fully solvated. The water O–H bond oscillators<sup>55,56</sup> can readily quench  $^1\text{O}_2$  to the ground state  $^3\text{O}_2$ , so that  $^1\text{O}_2$  migrates only ~150 nm as a solvated species. In the photoreactor, the unequal abstractions of surfactant methyl and methylene allylic hydrogens provided a further mechanistic handle.

We favor a mechanism shown in Figure 9A for the  $^1\text{O}_2$  “ene” reaction at the air–water interface. The following mechanisms depicted in Figure 9B–F are not consistent with our results: (i) attribution of regioselectivity to hyperconjugation<sup>57</sup> of the alkene head is unlikely due to high energetics for C–C bond/no-bond resonance, (ii and iii) implicit water via electronic repulsion to the peroxide is unlikely because O–H bonds and not lone pair electrons situate themselves vertically,<sup>58</sup> or

the water interface as a “large” substituent is unlikely as it would preferentially lead to the 3° hydroperoxide, not the 2° hydroperoxide, as observed, (iv and v) specific water interactions via anchimeric assistance or H-bonding to the perepoxide are unlikely in which the 3° hydroperoxide would be preferred, and not the 2° hydroperoxide, and higher percent yields for shorter surfactant in the series, both opposite to what was observed. The proposed mechanism is shown in Figure 9A, in which the water layer functions as a physical quencher of the approaching  $^1\text{O}_2$  is thus proposed as the most likely mechanism, as seen in Figure 2 (eq 3). Vibrational physical quenching of  $^1\text{O}_2$  by water is pertinent here, as reported previously.<sup>55,56,59–61</sup> Pertinent here is the higher yield and greater selectivity in the longer chain 11C as it minimizes contact between the prenyl group and water, for preferential allylic hydrogen abstraction of the methyl groups by airborne  $^1\text{O}_2$ . The methylene allylic hydrogens are less accessible (closer to the physically quenching water surface), making methyl hydrogen abstraction favorable to reach the 2° hydroperoxide.

The importance of the surfactant chain length is similarly corroborated by an increase in the regioselectivity of the 2° ROOH in longer 11C compared to the shorter 9C and 7C. Singlet oxygen is a longer-lived species in the gas phase for arrival at the surface for an increase in selectivity as the chain length increases from 7C to 9C then to 11C (from 2.5:1 to 3.2:1). This pattern might reflect a greater aqueous layer influence in the shorter chain surfactants, and accompanying reduction in regioselectivity, which reduces even further in the  $^1\text{O}_2$  bubbler. For the  $^1\text{O}_2$  bubbler, the regioselectivity nearly disappears, even for the long-chain 11C surfactant (Figure 9G).

This led us to ask the question: *How does the work fit in the field of organic oxidation selectivity?* The work improves the state-of-the-art because the delivery of  $^1\text{O}_2$  from mainly a dry or wet origin can tune the selectivity from high to low. A mechanistic picture is available for turning off regioselectivity in the hydrogen abstraction step of  $^1\text{O}_2$  with alkene surfactants. In the photoreactor, surfactant molecules are evenly dispersed on the water surface and reside at the interface. In the bubble reactor, dynamic sparging results, where the attack of  $^1\text{O}_2$  on surfactant molecules arises in a higher solvated state, and thus regioselectivity is lost, in contrast to the situation with the photoreactor.

**Summary.** Many studies have focused on  $^1\text{O}_2$  chemistry in the solution phase or the gas phase, but sparingly few have focused on  $^1\text{O}_2$  at the air–water interface, in part due to the need to develop surface-active compounds. Furthermore, reactors for  $^1\text{O}_2$  generation and reactions in water have yet untapped potential.<sup>17</sup> To make inroads in this vein, two methods and three alkene surfactants (7C, 9C, and 11C) were used to probe the  $^1\text{O}_2$  “ene” reaction at the air–water interface. DFT-computed results point to solvation differences in a continuum from the gas-phase perepoxide TSs with low binding strengths to the solution-phase perepoxide intermediates with higher binding energies. With the alkene site located further away from the aqueous interface, this harkens us back to the old adage: *location, location, location*. A mechanism is proposed that explains how physically isolated  $^1\text{O}_2$  and solution-phase  $^1\text{O}_2$  affect the “ene” reaction with tunability for the range of perepoxide as a TS to an intermediate. The positioning of the alkene site is key, where regions emerge that controllably react the alkene with dry or wet  $^1\text{O}_2$ .

## CONCLUSIONS

A photoreactor and bubble reactor were used to provide mechanistic insights into which  $^1\text{O}_2$  was directionally trapped at the air–water interface. These reactors contained no photosensitizer in solution, which was advantageous for enabling singlet oxygen’s reactivity to be assessed without intervening species from type I photooxidation reactions. The use of the photo- and bubble reactors for the generation of  $^1\text{O}_2$  in alkene oxidations led to the “ene” reaction of  $^1\text{O}_2$  and the formation of a secondary and tertiary hydroperoxide at the air–water interface. Mechanistic evidence is provided for a continuum of the perepoxide ranging from a TS to an intermediate. Future studies could focus on deuterium labeling one of the two geminal methyl groups for further insight into the regioselectivity of the  $^1\text{O}_2$  “ene” reaction under the two experimental conditions described in this study. Future studies could also be undertaken including enhanced selective oxidation reactions, further control of the perepoxide TS and intermediate continuum, and comparison of the surface area exposed to air with high and low surfactant packing at the air–water interface.

Control of  $^1\text{O}_2$  chemistry at the air–water interface and the airborne state can make the photoreactor and bubble reactor methods advantageous to other methods, such as structure constraints (i.e., inaccessible allylic H) or homogeneous solutions.<sup>29–31</sup> The tuning of the  $^1\text{O}_2$  “ene” process with  $^1\text{O}_2$  as a gaseous species or partially aqueous solvated species makes these methods relevant for mechanistic control by the air–solution interface and fate of the  $^1\text{O}_2$  reaction. Such interfacial  $^1\text{O}_2$  control and mechanism is relevant in air, and oxidative damage, and adds to recent work focusing on other ROS such as HO• and ozone at an air–water interface.<sup>62–67</sup> The impact of the work goes beyond organic chemistry and is related to biologically relevant models of  $^1\text{O}_2$  at the membrane or marine aerosol surfaces.

## ASSOCIATED CONTENT

### Supporting Information

The Supporting Information is available free of charge at <https://pubs.acs.org/doi/10.1021/acs.langmuir.2c00279>.

Instrumentation and analysis methods; calculation of water layer surface-to-volume (S/V) ratios; an example of the  $^1\text{O}_2$  phosphorescence decay trace; and DFT-computed energies and geometries of stationary points of structures (PDF)

## AUTHOR INFORMATION

### Corresponding Authors

Jianbo Liu – Department of Chemistry and Biochemistry, Queens College of the City University of New York, Queens, New York 11367, United States; Ph.D. Program in Chemistry, The Graduate Center of the City University of New York, New York, New York 10016, United States; [orcid.org/0000-0001-9577-3740](https://orcid.org/0000-0001-9577-3740); Email: [Jianbo.Liu@qc.cuny.edu](mailto:Jianbo.Liu@qc.cuny.edu)

Alexander Greer – Department of Chemistry, Brooklyn College of the City University of New York, Brooklyn, New York 11210, United States; Ph.D. Program in Chemistry, The Graduate Center of the City University of New York, New York, New York 10016, United States; [orcid.org/0000-0003-4444-9099](https://orcid.org/0000-0003-4444-9099); Email: [AGreer@brooklyn.cuny.edu](mailto:AGreer@brooklyn.cuny.edu)

## Authors

**Belaid Malek** – Department of Chemistry, Brooklyn College of the City University of New York, Brooklyn, New York 11210, United States

**Wenchao Lu** – Department of Chemistry and Biochemistry, Queens College of the City University of New York, Queens, New York 11367, United States; Ph.D. Program in Chemistry, The Graduate Center of the City University of New York, New York, New York 10016, United States; [orcid.org/0000-0002-3798-5128](https://orcid.org/0000-0002-3798-5128)

**Prabhu Prasad Mohapatra** – Department of Chemistry, Brooklyn College of the City University of New York, Brooklyn, New York 11210, United States; Ph.D. Program in Chemistry, The Graduate Center of the City University of New York, New York, New York 10016, United States; [orcid.org/0000-0002-6707-048X](https://orcid.org/0000-0002-6707-048X)

**Niluksha Walalawela** – Department of Chemistry, Brooklyn College of the City University of New York, Brooklyn, New York 11210, United States; Ph.D. Program in Chemistry, The Graduate Center of the City University of New York, New York, New York 10016, United States; [orcid.org/0000-0002-6739-5049](https://orcid.org/0000-0002-6739-5049)

**Shakeela Jabeen** – Department of Chemistry, Brooklyn College of the City University of New York, Brooklyn, New York 11210, United States; Ph.D. Program in Chemistry, The Graduate Center of the City University of New York, New York, New York 10016, United States; [orcid.org/0000-0002-7153-3379](https://orcid.org/0000-0002-7153-3379)

Complete contact information is available at:

<https://pubs.acs.org/10.1021/acs.langmuir.2c00279>

## Notes

The authors declare no competing financial interest.

## ACKNOWLEDGMENTS

B.M., P.P.M., N.W., S.J., and A.G. acknowledge support from the National Science Foundation (CHE-1856765). W.L. and J.L. acknowledge the support by the National Science Foundation (Grant No. CHE-1856362). This work used Comet and Expanse, in the Extreme Science and Engineering Discovery Environment (XSEDE) cluster at the San Diego Supercomputer Center, which is supported by the NSF (ACI-1548562) through allocation CHE-210052. We also thank Leda Lee for assistance with the graphic arts work.

## REFERENCES

- (1) Griesbeck, A. G.; Goldfuss, B.; Jager, C.; Brullingen, E.; Lippold, T.; Kleczka, M. Strong Asymmetry in the Peroxide Bifurcation Mechanism: The Large-Group Effect in the Singlet Oxygen Ene Reaction with Allylic Alcohols. *ChemPhotoChem* **2017**, *1*, 213–221.
- (2) Ess, D. H.; Wheeler, S. E.; Iafe, R. G.; Xu, L.; Çelebi-Ol0çum, N.; Houk, K. N. Bifurcations on Potential Energy Surfaces of Organic Reactions. *Angew. Chem., Int. Ed. Engl.* **2008**, *47*, 7592–7601.
- (3) Singleton, D. A.; Hang, C.; Szymanski, M. J.; Meyer, M. P.; Leach, A. G.; Kuwata, K. T.; Chen, J. S.; Greer, A.; Foote, C. S.; Houk, K. N. Mechanism of Ene Reactions of Singlet Oxygen. A Two-Step No-Intermediate Mechanism. *J. Am. Chem. Soc.* **2003**, *125*, 1319–1328.
- (4) Ortega, T.; Ozer, G.; Gronert, S.; Erden, I. Singlet Oxygenation of Triquinacene, Barrelene, and Homobarrelene. *Tetrahedron Lett.* **2020**, *61*, No. 151779.
- (5) Alberti, M. N.; Orfanopoulos, M. Unraveling the Mechanism of the Singlet Oxygen Ene Reaction: Recent Computational and Experimental Approaches. *Chem. – Eur. J.* **2010**, *16*, 9414–9421.
- (6) Sheppard, A. N.; Acevedo, O. Multidimensional Exploration of Valley–Ridge Inflection Points on Potential-Energy Surfaces. *J. Am. Chem. Soc.* **2009**, *131*, 2530–2540.
- (7) Alberti, M. N.; Orfanopoulos, M. The Cyclopropyl Group as a Hypersensitive Probe in the Singlet Oxygen Ene Reaction Mechanism. *Org. Lett.* **2008**, *10*, 2465–2468.
- (8) Grdina, M. B.; Orfanopoulos, M.; Stephenson, L. M. Stereochemical Dependence of Isotope Effects in the Singlet Oxygen-Olefin Reaction. *J. Am. Chem. Soc.* **1979**, *101*, 3111–3112.
- (9) Baptista, M. S.; Cadet, J.; Di Mascio, P.; Ghogare, A. A.; Greer, A.; Hamblin, M. R.; Lorente, C.; Nunez, S. C.; Ribeiro, M. S.; Thomas, A. H.; Vignoni, M.; Yoshimura, T. M. Type I and Type II Photosensitized Oxidation Reactions: Guidelines and Mechanistic Pathways. *Photochem. Photobiol.* **2017**, *93*, 912–919.
- (10) Baptista, M. S.; Cadet, J.; Greer, A.; Thomas, A. H. Photosensitization Reactions of Biomolecules: Definition, Targets, and Mechanisms. *Photochem. Photobiol.* **2021**, *97*, 1456–1483.
- (11) Ramamurthy, V.; Sivaguru, J. Supramolecular Photochemistry as a Potential Synthetic Tool: Photocycloaddition. *Chem. Rev.* **2016**, *116*, 9914–9993.
- (12) Sivaguru, J.; Natarajan, A.; Kaanumalle, L. S.; Shailaja, J.; Uppili, S.; Joy, A.; Ramamurthy, V. Asymmetric Photoreactions within Zeolites: Role of Confinement and Alkali Metal Ions. *Acc. Chem. Res.* **2003**, *36*, 509–521.
- (13) Cojocar, B.; Laferrière, M.; Carbonell, E.; Parvulescu, V.; Garcia, H.; Scaiano, J. C. Direct Time-Resolved Detection of Singlet Oxygen in Zeolite-Based Photocatalysts. *Langmuir* **2008**, *24*, 4478–4481.
- (14) Li, X.; Ramamurthy, V. Selective Oxidation of Olefins within Organic Dye Cation-Exchanged Zeolites. *J. Am. Chem. Soc.* **1996**, *118*, 10666–10667.
- (15) Tonon, C. C.; Ashraf, S.; Alburquerque, J. Q.; de Sousa, N.; Rastelli, A.; Hasan, T.; Lyons, A. M.; Greer, A. Antimicrobial Photodynamic Inactivation Using Topical and Superhydrophobic Sensitizer Techniques: A Perspective from Diffusion in Biofilms. *Photochem. Photobiol.* **2021**, *97*, 1266–1277.
- (16) Durantini, A. M.; Greer, A. Interparticle Delivery and Detection of Volatile Singlet Oxygen at Air/solid Interfaces. *Environ. Sci. Technol.* **2021**, *55*, 3559–3567.
- (17) Jeyapalan, V.; Varadharajan, R.; Veerakanellore, G. B.; Ramamurthy, V. Water: An Underappreciated Reaction Medium for Photodimerizations. *J. Photochem. Photobiol., A* **2021**, *420*, 113492.
- (18) Geng, W.-C.; Zhang, D.; Gong, C.; Li, Z.; Barraza, K. M.; Beauchamp, J. L.; Guo, D.-S.; Zhang, X. Host–Guest Complexation of Amphiphilic Molecules at the Air–Water Interface Prevents Oxidation by Hydroxyl Radicals and Singlet Oxygen. *Angew. Chem., Int. Ed.* **2020**, *59*, 12684–12688.
- (19) Mu, C.; Wang, J.; Barraza, K. M.; Zhang, X.; Beauchamp, J. L. Mass Spectrometric Study of Acoustically Levitated Droplets Illuminates Molecular-Level Mechanism of Photodynamic Therapy for Cancer Involving Lipid Oxidation. *Angew. Chem., Int. Ed.* **2019**, *58*, 8082–8086.
- (20) Zhang, X.; Barraza, K. M.; Upton, K. T.; Beauchamp, J. L. Subtle Changes in Lipid Environment Have Profound Effects on Membrane Oxidation Chemistry. *J. Am. Chem. Soc.* **2018**, *140*, 17492–17498.
- (21) Zhang, X.; Barraza, K. M.; Beauchamp, J. L. Cholesterol Provides Nonsacrificial Protection of Membrane Lipids from Chemical Damage at Air–Water Interface. *Proc. Natl. Acad. Sci. U. S. A.* **2018**, *115*, 3255–3260.
- (22) Huang, Y.; Barraza, K. M.; Kenseth, C. M.; Zhao, R.; Wang, C.; Beauchamp, J. L.; Seinfeld, J. H. Probing the OH Oxidation of Pinonic Acid at the Air–Water Interface Using Field-Induced Droplet Ionization Mass Spectrometry (FIDI-MS). *J. Phys. Chem. A* **2018**, *122*, 6445–6456.
- (23) Anglada, J. M.; Martins-Costa, M. T. C.; Francisco, J. S.; Ruiz-López, M. F. Photoinduced Oxidation Reactions at the Air–Water Interface. *J. Am. Chem. Soc.* **2020**, *142*, 16140–16155.

- (24) Martins-Costa, M. T. C.; Anglada, J. M.; Francisco, J. S.; Ruiz-López, M. F. Photochemistry of SO<sub>2</sub> at the Air–Water Interface: A Source of OH and HOSO Radicals. *J. Am. Chem. Soc.* **2018**, *140*, 12341–12344.
- (25) Zhang, D.; Gong, C.; Wang, J.; Mu, C.; Wang, W.; Zhang, X. Beyond Lipid Peroxidation: Distinct Mechanisms Observed for POPC and POPG Oxidation Initiated by UV-Enhanced Fenton Reactions at the Air–Water Interface. *J. Mass Spectrom.* **2020**, *56*, e4626.
- (26) Eugene, A. J.; Guzman, M. I. Production of Singlet Oxygen (<sup>1</sup>O<sub>2</sub>) during the Photochemistry of Aqueous Pyruvic Acid: The Effects of pH and Photon Flux under Steady-State O<sub>2(aq)</sub> Concentration. *Environ. Sci. Technol.* **2019**, *53*, 12425–12432.
- (27) Pillar, E. A.; Guzman, M. I. Oxidation of Substituted Catechols at the Air–Water Interface: Production of Carboxylic Acids, Quinones, and Polyphenols. *Environ. Sci. Technol.* **2017**, *51*, 4951–4959.
- (28) Anglada, J. M.; Martins-Costa, M.; Ruiz-López, M. F.; Francisco, J. S. Spectroscopic Signatures of Ozone at the Air–Water Interface and Photochemistry Implications. *Proc. Natl. Acad. Sci. U. S. A.* **2014**, *111*, 11618–11623.
- (29) Poon, T. H. W.; Pringle, K.; Foote, C. S. Reaction of Cyclooctenes with Singlet Oxygen. Trapping of a Peroxide Intermediate. *J. Am. Chem. Soc.* **1995**, *117*, 7611–7618.
- (30) Leach, A. G.; Houk, K. N.; Foote, C. S. Theoretical Prediction of a Peroxide Intermediate for the Reaction of Singlet Oxygen with *trans*-Cyclooctene Contrasts with the Two-Step No-Intermediate Ene Reaction for Acyclic Alkenes. *J. Org. Chem.* **2008**, *73*, 8511–8519.
- (31) Turque, O.; Greer, A.; Wauchope, O. R. Synthetic Feasibility of Oxygen-Driven Photoisomerizations of Alkenes and Polyenes. *Org. Biomol. Chem.* **2020**, *18*, 9181–9190.
- (32) Kwon, B.-M.; Foote, C. S.; Khan, S. I. Chemistry of Singlet Oxygen. 52. Reaction with *trans*-Stilbene. *J. Org. Chem.* **1989**, *54*, 3378–3382.
- (33) Shimizu, N.; Bartlett, P. D. Photooxidation of Olefins Sensitized by  $\alpha$ -Diketones and by Benzophenone. A Practical Epoxidation Method with Biacetyl. *J. Am. Chem. Soc.* **1976**, *98*, 4193–4200.
- (34) Maranzana, A.; Ghigo, G.; Tonachini, G. Mechanistic Significance of Peroxide Trapping Experiments, with Epoxide Detection, in <sup>1</sup>Δ<sub>g</sub> Dioxygen Reactions with Alkenes. *J. Org. Chem.* **2003**, *68*, 3125–3129.
- (35) Malek, B.; Fang, W.; Abramova, I.; Walalawela, N.; Ghogare, A. A.; Greer, A. 'Ene' Reactions of Singlet Oxygen at the Air–Water Interface. *J. Org. Chem.* **2016**, *81*, 6395–6401.
- (36) Fang, Y.; Liu, F.; Bennett, A.; Ara, S.; Liu, J. Experimental and Trajectory Study on the Reaction of Protonated Methionine with Electronically Excited Singlet Molecular Oxygen (<sup>1</sup>Δ<sub>g</sub>): Reaction Dynamics and Collision Energy Effects. *J. Phys. Chem. B* **2011**, *115*, 2671–2682.
- (37) Liu, F.; Lu, W.; Yin, X.; Liu, J. Mechanistic and Kinetic Study of Singlet O<sub>2</sub> Oxidation of Methionine by On-Line Electrospray Ionization Mass Spectrometry. *J. Am. Soc. Mass Spectrom.* **2016**, *27*, 59–72.
- (38) Lafferty, W. J.; Solodov, A. M.; Lugez, C. L.; Fraser, G. T. Rotational Line Strengths and Self-Pressure-Broadening Coefficients for the 1.27- $\mu$ m, <sup>1</sup>Δ<sub>g</sub> → X<sub>3</sub>Σ<sub>g</sub><sup>-</sup>,  $\nu = 0-0$  band of O<sub>2</sub>. *Appl. Opt.* **1998**, *37*, 2264–2270.
- (39) Skovsen, E.; Snyder, J. W.; Lambert, J. D. C.; Ogilby, P. R. Lifetime and Diffusion of Singlet Oxygen in a Cell. *J. Phys. Chem. B* **2005**, *109*, 8570–8573.
- (40) Zamadar, M.; Aebisher, D.; Greer, A. Singlet Oxygen Delivery Through the Porous Cap of a Hollow-Core Fiber Optic Device. *J. Phys. Chem. B* **2009**, *113*, 15803–15806.
- (41) Lindig, B. A.; Rodgers, M. A. J.; Schaap, A. P. Determination of the Lifetime of Singlet Oxygen in Water-D<sub>2</sub> Using 9,10-Anthracene-dipropionic Acid, a Water-Soluble Probe. *J. Am. Chem. Soc.* **1980**, *102*, 5590–5593.
- (42) Alecu, I. M.; Zheng, J.; Zhao, Y.; Truhlar, D. G. Computational Thermochemistry: Scale Factor Databases and Scale Factors for Vibrational Frequencies Obtained from Electronic Model Chemistries. *J. Chem. Theory Comput.* **2010**, *6*, 2872–2887.
- (43) Marenich, A. V.; Cramer, C. J.; Truhlar, D. G. Universal Solvation Model Based on Solute Electron Density and on a Continuum Model of the Solvent Defined by the Bulk Dielectric Constant and Atomic Surface Tensions. *J. Phys. Chem. B* **2009**, *113*, 6378–6396.
- (44) Maranzana, A.; Ghigo, G.; Tonachini, G. Diradical and Peroxirane Pathways in the [ $\pi_2 + \pi_2$ ] Cycloaddition Reactions of <sup>1</sup>Δ<sub>g</sub> Dioxygen with Ethene, Methyl Vinyl Ether, and Butadiene: A Density Functional and Multireference Perturbation Theory Study. *J. Am. Chem. Soc.* **2000**, *122*, 1414–1423.
- (45) Benny, J.; Saito, T.; Moe, M. M.; Liu, J. Singlet O<sub>2</sub> Reactions with Radical Cations of 8-Bromoguanine and 8-Bromoguanosine: Guided-Ion Beam Mass Spectrometric Measurements and Theoretical Treatments. *J. Phys. Chem. A* **2022**, *126*, 68–79.
- (46) Lee, T. J.; Taylor, P. R. A Diagnostic for Determining the Quality of Single-Reference Electron Correlation Methods. *Int. J. Quantum Chem., Quantum Chem. Symp.* **1989**, *36*, 199–207.
- (47) Liakos, D. G.; Sparta, M.; Kesharwani, M. K.; Martin, J. M. L.; Neese, F. Exploring the Accuracy Limits of Local Pair Natural Orbital Coupled-Cluster Theory. *J. Chem. Theory Comput.* **2015**, *11*, 1525–1539.
- (48) Frisch, M. J.; Trucks, G. W.; Schlegel, H. B.; Scuseria, G. E.; Robb, M. A.; Cheeseman, J. R.; Scalmani, G.; Barone, V.; Mennucci, B.; Petersson, G. A.; et al. *Gaussian 09, Rev. D.01*, Gaussian, Inc.; Wallingford, CT, 2013.
- (49) Neese, F. Software Update: The ORCA Program System, Version 4.0. *WIREs Comput. Mol. Sci.* **2018**, *8*, e1327.
- (50) Choudhury, R.; Greer, A. Synergism between Airborne Singlet Oxygen and a Trisubstituted Olefin Sulfonate for the Inactivation of Bacteria. *Langmuir* **2014**, *30*, 3599–3605.
- (51) Jabeen, S.; Farag, M.; Malek, B.; Choudhury, R.; Greer, A. A Singlet Oxygen Priming Mechanism: Disentangling of Photooxidative and Downstream Dark Effects. *J. Org. Chem.* **2020**, *85*, 12505–12513.
- (52) Bartusik, D.; Aebisher, D.; Lyons, A. M.; Greer, A. Bacterial Inactivation by a Singlet Oxygen Bubbler: Identifying Factors Controlling the Toxicity of <sup>1</sup>O<sub>2</sub> Bubbles. *Environ. Sci. Technol.* **2012**, *46*, 12098–12104.
- (53) Manring, L. E.; Foote, C. S. Chemistry of Singlet Oxygen. 44. Mechanism of Photooxidation of 2,5-Dimethylhexa-2,4-Diene and 2-Methyl-2-Pentene. *J. Am. Chem. Soc.* **1983**, *105*, 4710–4717.
- (54) Wilkinson, F.; Helman, W. P.; Ross, A. B. Quantum Yields for the Photosensitized Formation of the Lowest Electronically Excited Singlet State of Molecular Oxygen in Solution. *J. Phys. Chem. Ref. Data* **1995**, *24*, 663–677.
- (55) Poon, T.; Sivaguru, J.; Franz, R.; Jockusch, S.; Martinez, C.; Washington, I.; Adam, W.; Inoue, Y.; Turro, N. J. Temperature and Solvent Control of the Stereoselectivity in the Reactions of Singlet Oxygen with Oxazolidinone-Substituted Enecarbamates. *J. Am. Chem. Soc.* **2004**, *126*, 10498–10499.
- (56) Schweitzer, C.; Schmidt, R. Physical Mechanisms of Generation and Deactivation of Singlet Oxygen. *Chem. Rev.* **2003**, *103*, 1685–1758.
- (57) Alabugin, I. V.; Gomes, G. D. P.; Abdo, M. A. Hyperconjugation. *WIREs Comput. Mol. Sci.* **2019**, e1389.
- (58) Donaldson, D. J.; Valsaraj, K. T. Adsorption and Reaction of Trace Gas-Phase Organic Compounds on Atmospheric Water Film Surfaces: A Critical Review. *Environ. Sci. Technol.* **2010**, *44*, 865–873.
- (59) Sivaguru, J.; Solomon, M. R.; Poon, T.; Jockusch, S.; Bosio, S. G.; Adam, W.; Turro, N. J. The Reaction of Singlet Oxygen with Enecarbamates: A Mechanistic Playground for Investigating Chemo-selectivity, Stereoselectivity, and Vibratoselectivity of Photooxidations. *Acc. Chem. Res.* **2008**, *41*, 387–400.
- (60) Sivaguru, J.; Solomon, M. R.; Saito, H.; Poon, T.; Jockusch, S.; Adam, W.; Inoue, Y.; Turro, N. J. Conformationally Controlled (Entropy Effects), Stereoselective Vibrational Quenching of Singlet

Oxygen in the Oxidative Cleavage of Oxazolidinone-Functionalized Enecarbamates through Solvent and Temperature Variations. *Tetrahedron* **2006**, *62*, 6707–6717.

(61) Ghogare, A. A.; Greer, A. Using Singlet Oxygen to Synthesize Natural Products and Drugs. *Chem. Rev.* **2016**, *116*, 9994–10034.

(62) Rana, M. S.; Guzman, M. I. Oxidation of Phenolic Aldehydes by Ozone and Hydroxyl Radicals at the Air–Water Interface. *J. Phys. Chem. A* **2020**, *124*, 8822–8833.

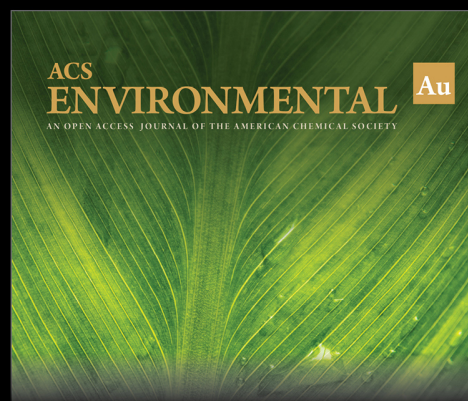
(63) Hayeck, N.; Mussa, I.; Perrier, S.; George, C. Production of Peroxy Radicals from the Photochemical Reaction of Fatty Acids at the Air–Water Interface. *ACS Earth Space Chem.* **2020**, *4*, 1247–1253.

(64) Anglada, J. M.; Martins-Costa, M.; Francisco, J. S.; Ruiz-López, M. F. Interconnection of Reactive Oxygen Species Chemistry across the Interfaces of Atmospheric, Environmental, and Biological Processes. *Acc. Chem. Res.* **2015**, *48*, 575–583.

(65) Enami, S.; Hoffmann, M. R.; Colussi, A. J. *In situ* Mass Spectrometric Detection of Interfacial Intermediates in the Oxidation of  $\text{RCOOH}_{(\text{aq})}$  by Gas-Phase OH-Radicals. *J. Phys. Chem. A* **2014**, *118*, 4130–4137.

(66) Martins-Costa, M. T. C.; Anglada, J. M.; Francisco, J. S.; Ruiz-Lopez, M. F. Reactivity of Atmospherically Relevant Small Radicals at the Air–Water Interface. *Angew. Chem., Int. Ed. Engl.* **2012**, *51*, 5413–5417.

(67) Thompson, K. C.; Rennie, A. R.; King, M. D.; Hardman, S. J. O.; Lucas, C. O. M.; Pfrang, C.; Hughes, B. R.; Hughes, A. V. Reaction of a Phospholipid Monolayer with Gas-Phase Ozone at the Air–Water Interface: Measurement of Surface Excess and Surface Pressure in Real Time. *Langmuir* **2010**, *26*, 17295–17303.



Editor-in-Chief: **Prof. Shelley D. Minteer**, University of Utah, USA



Deputy Editor:

**Prof. Xiang-Dong Li**

Hong Kong Polytechnic University, China

**Open for Submissions** 

pubs.acs.org/environau

 **ACS Publications**  
Most Trusted. Most Cited. Most Read.